IOP PUBLISHING NANOTECHNOLOGY
Nanotechnology **18** (2007) 155305 (7pp) doi:10.1088/0957-4484/18/15/155305

Multifunctional carbon nanotubes with nanoparticles embedded in their walls

D Mattia[1], G Korneva[2], A Sabur[1], G Friedman[3] and Y Gogotsi[1,4]

[1] Materials Science and Engineering Department and A J Drexel Nanotechnology Institute, Drexel University, 3141 Chestnut Street, Philadelphia, PA 19104, USA
[2] Chemistry Department, Drexel University, 3141 Chestnut Street, Philadelphia, PA 19104, USA
[3] Electrical and Computer Engineering Department, Drexel University, 3141 Chestnut Street, Philadelphia, PA 19104, USA

E-mail: gogotsi@drexel.edu

Received 18 December 2006, in final form 26 January 2007
Published 9 March 2007
Online at stacks.iop.org/Nano/18/155305

Abstract
Controlled amounts of nanoparticles ranging in size and composition were embedded in the walls of carbon nanotubes during a template-assisted chemical vapour deposition (CVD) process. The encapsulation of gold nanoparticles enabled surface enhanced Raman spectroscopy (SERS) detection of glycine inside the cavity of the nanotubes. Iron oxide particles are partially reduced to metallic iron during the CVD process giving the nanotubes ferromagnetic behaviour. At high nanoparticle concentrations, particle agglomerates can form. These agglomerates or larger particles, which are only partially embedded in the walls of the nanotubes, are covered by additional carbon layers inside the hollow cavity of the tube producing hillocks inside the nanotubes, with sizes comparable to the bore of the tube.

S Supplementary data are available from stacks.iop.org/Nano/18/155305

1. Introduction

Decoration of the walls of carbon nanotubes (CNTs) [1] with functional groups [2] and/or nanoparticles has been performed to add additional functionality to CNTs. In recent years, decoration of CNTs has been used to increase the hydrogen storage capacity [3], to make nanotubes magnetic [4], or to grow secondary structures inside the nanotubes to increase the available surface for catalysis [5]. Functionalization of the interior walls of carbon nanotubes, in particular those produced using a non-catalytic template-assisted chemical vapour deposition (CVD) method, has been achieved using different methods, such as direct fluorination [6] or nitric acid treatment [7], or filling with magnetic [8] and fluorescent [9] nanoparticles.

Nanotubes with inner diameters from tens to hundreds of nanometres are promising candidates for cellular probes. These will require not only control over mechanical and electrical properties, but also added functionality that will enable their magnetic manipulation, which is safe for live cells and tissue. Incorporation of particles that produce plasmon resonance and enable surface enhanced Raman spectroscopy study of cells with single-molecule sensitivity would also be beneficial.

The presence of particles inside nanotubes, assuming they do not block the tube channel completely, may be beneficial in nanofluidic devices. Fluid mixing currently represents an obstacle to the development of functional microfluidic and nanofluidic devices. It has been shown that fluid flow in nanochannels is laminar [10]. As a result, fluid mixing in a narrow channel is very difficult. Complex microfluidic circuits have been designed to solve this problem, but all involve valves or some kind of actuation [11], which is very difficult to incorporate into nanotube-based nanofluidic devices [12].

In this work, we investigate the synthesis and applications of multifunctional nanotubes with controllable amounts of nanoparticles embedded in their walls during the CVD synthesis process. Different kinds of nanoparticles have been used to add different functionalities to the resulting nanotubes by producing nanostructures within the walls or inside tube channels without altering the chemistry of the nanotube surfaces.

[4] Author to whom any correspondence should be addressed.

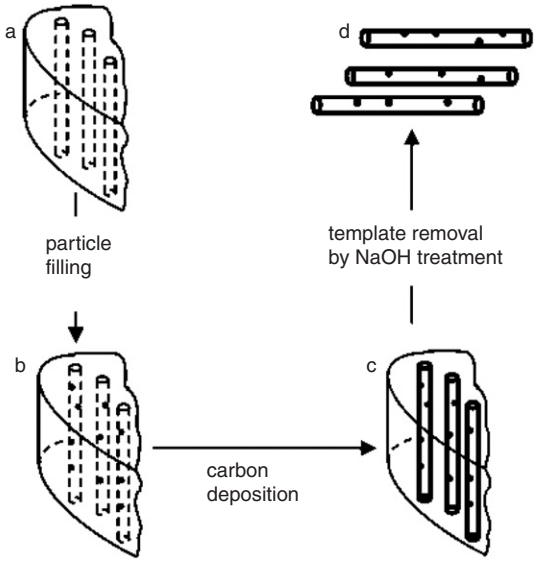

Figure 1. Schematic diagrams of the synthesis of CVD-nanotubes with nanoparticles embedded in the walls: (a) an empty membrane is (b) filled with nanoparticles immersed in an acidic solution. (c) Nanotubes are deposited inside the pores of the membrane through CVD. (d) Free-standing CNTs with particles embedded in the walls are obtained after dissolution of the membrane.

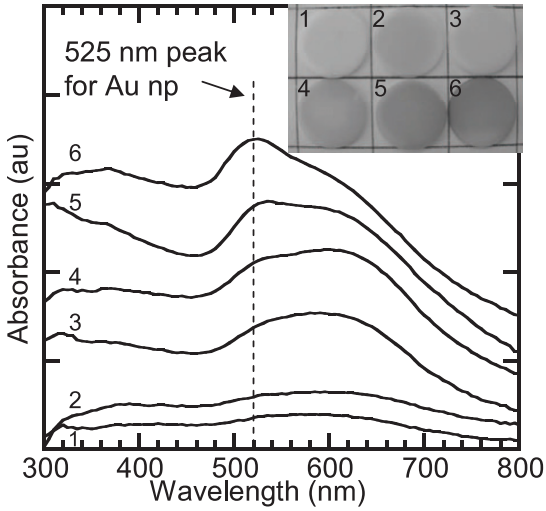

Figure 2. UV–vis spectra of alumina membranes after immersion in acid solutions (pH ∼ 5) with increasing concentration of Au nanoparticles. Spectra 1 to 6 correspond to 0.025, 0.05, 0.125, 0.25, 0.375, and 0.5 ml of nanoparticle solution in 10 ml of H_2O, respectively. The inset shows the actual membranes with a diameter of 13 mm.

2. Materials and methods

Gold nanoparticles were prepared by mixing 20 ml of 1 mM solution of hydrochloroauric acid (hydrogen tetrachloroaurate) with 1 ml of 1% trisodium citrate ($Na_3C_6H_5O_7{\cdot}2H_2O$) at boiling temperature with vigorous stirring [13, 14]. The particles had a diameter of 10–30 nm, comparable or slightly larger than the average wall thickness of CVD-nanotubes. Iron oxide nanoparticles (Fe_3O_4, average diameter 10 nm, density 1070 kg m^{-3}) were delivered from an aqueous ferrofluid solution (EMG 508 from Ferrotec Corporation, 1.2 vol% of particles in aqueous solution) [8].

The nanotube synthesis process is based on the well known non-catalytic CVD template-assisted approach [15]. Anodized aluminium oxide membranes, used as templates for CNT growth, were produced with pore diameters ranging from 20 to 200 nm and with lengths up to 90 μm. Details of the template synthesis have been reported elsewhere [16, 17].

For each type of nanoparticle, the templates were immersed in 10 ml acidic solutions, with pH 5 for Au and pH 6 for Fe_3O_4 nanoparticles (figure 1(a)). Subsequently, from 0.005 to 1.0 ml of concentrated nanoparticle colloid was added to each solution. In an acidic environment, the alumina template will have a slightly positive charge, thus negatively charged nanoparticles will adhere electrostatically to the template (figure 1(b)). After 24 h, the templates were rinsed on filter paper to remove the excess solution, leaving the templates with a controlled amount of particles. CVD was performed at 670 °C for 6 h using ethylene as a carbon source (figure 1(c)) [18]. Upon removal of the template in boiling 1 M NaOH solution (3 h in refluxing conditions), free-standing, open-ended, straight nanotubes with nanoparticles embedded in the walls were obtained (figure 1(d)). The resulting nanotubes have a disordered carbon wall structure with an average in-plane graphite crystallite size of 2.5 nm [16, 17].

The samples were characterized by transmission electron microscopy (TEM) using a JEOL JEM-2010F coupled with an energy dispersive x-ray spectroscopy (EDS) detector from EDAX, and by environmental scanning electron microscopy (Zeiss SUPRA LV). The magnetic properties of the nanotubes filled with iron oxide particles were measured at room temperature using an alternating gradient magnetometer (Princeton Measurements Corporation). In the regions below −2.5 kOe and above 2.5 kOe, data points were collected every 100 Oe; inside this interval, points were collected every 3 Oe to increase data accuracy in the hysteresis region.

X-ray diffraction (XRD) patterns were recorded using a Siemens XRD with Cu Kα source. Surface enhanced Raman spectra were recorded using a Raman micro-spectrometer (Renishaw 1000) and a diode laser (785 nm excitation wavelength). UV/vis spectra on solid samples were taken with a Perkin Elmer UV/vis/NIR spectrophotometer Lambda 950 equipped with a 60 mm integrating sphere.

3. Results and discussion

3.1. Nanotube morphology and structure

UV–vis absorption spectra of membranes, immersed in solutions with increasing Au nanoparticle concentration, show an increase in the peak for gold at 525 nm (figure 2). Thus, it is possible to control the amount of particles embedded in the walls of the nanotubes.

SEM micrographs of fractured nanotubes show an external smooth shell and an internal wall characterized by the presence of hillocks or bumps with a low density of particles (figure 3(a), 0.025 ml Au np solution) or a high density, uniform distribution of particles (figure 3(b), 0.25 ml of Au np solution). These 'bumps' can only be due to the presence of the nanoparticles, because the average in-plane graphite crystallite size of

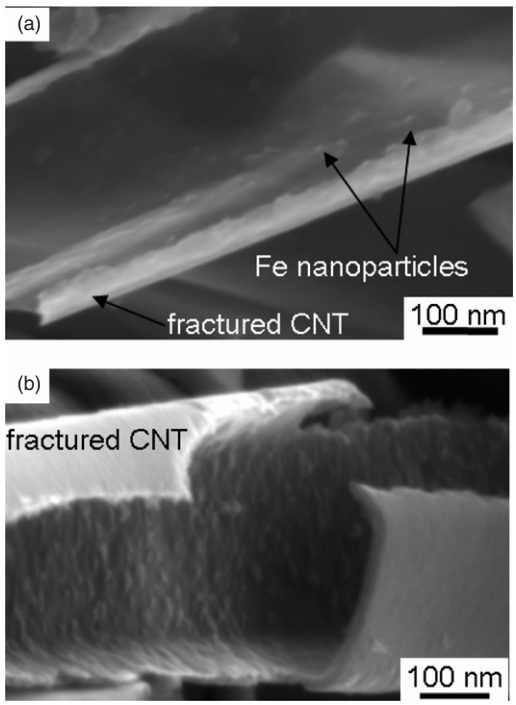

Figure 3. SEM micrographs of fractured nanotubes with an outer, smooth shell and an internal shell with (a) low density of Fe nanoparticles and (b) high density, uniform distribution of Au nanoparticles.

2.5 nm [16] is too small to account for surface roughness in the order of tens of nanometres. The external wall, which replicates the pore surface, appears smooth at the magnification used in figure 3. TEM analysis indeed confirms this hypothesis, showing, for example, a FeC-based nanoparticle completely surrounded by carbon (figure 4(a)). A higher resolution TEM image further confirms that the particle is embedded in the wall and does not sit on the tube surface by showing carbon grown around a gold particle, with both the carbon and the crystal lattice of the metal particle being in focus at the same time (figure 4(b)). The composition of the Au particle was confirmed by EDS (not shown).

Annealing for 2 h at 2000 °C in vacuum (10^{-6} Torr), caused the CVD CNT nanotube to graphitize, forming an ordered graphitic MWNT [16]. This process causes the evaporation of the metallic particles, while the carbon structure covering the nanoparticle is retained (figure 4(c)). This further confirms that the particles are embedded in the walls of the tube. Interestingly, the thickness of this curved carbon covering the exposed portion of the particle is approximately the same as of the nanotube wall.

When the higher concentrations of particle colloid are used, agglomerates may form, which are not completely embedded in the walls but protrude inside the hollow cavity of the tube (as in figure 3). The exposed surface is covered by CVD carbon, with the formation of hillocks, with sizes comparable to the bore of the nanotube (figure 4(d)).

In the case of ferrofluid, nanoparticles that were not completely embedded in the walls of the CVD tubes acted as catalysts for the growth of small (20–30 nm in diameter) MWNTs (see figure S1 in the supplementary information

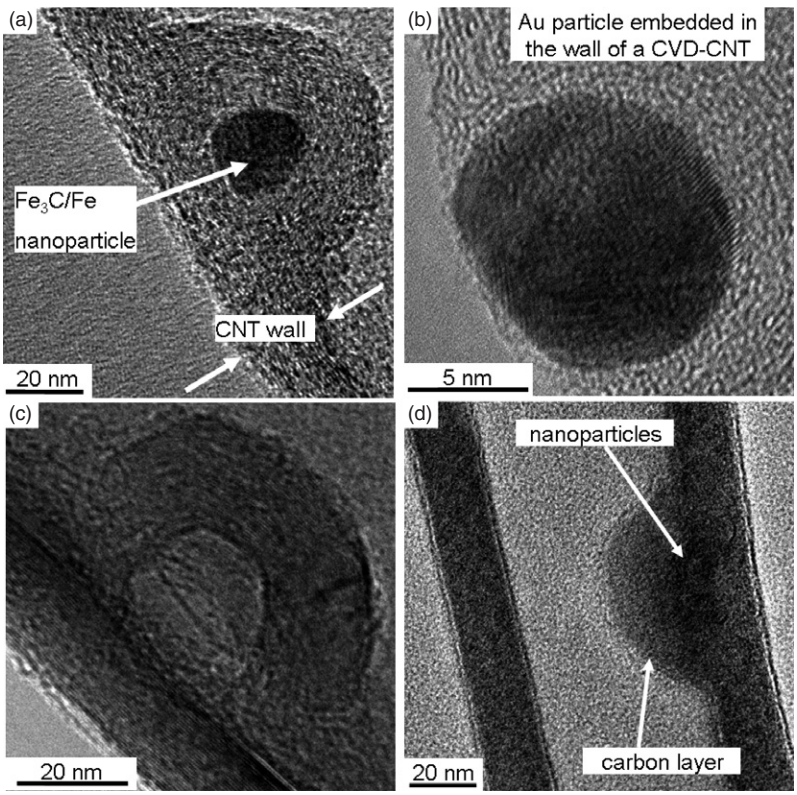

Figure 4. TEM micrographs of particles embedded in CNT walls: (a) Fe and (b) Au nanoparticles. (c) Empty cavity after evaporation of the Au particle during annealing. (d) Hillock grown around an aggregate of particles inside the cavity of a CVD-CNT.

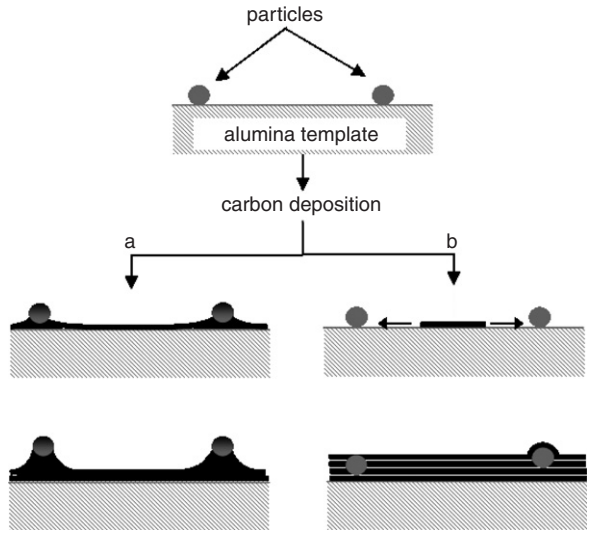

Figure 5. Growth mechanisms for CNTs with particles embedded in the walls: (a) tip-growth mechanism, with particles lifted from the membrane pore wall due to the formation of a metal carbide particle and further dissolution of carbon in the carbide with subsequent lift of the particle. (b) Carbon first deposits on the alumina and forms a continuous layer due to the faster growth kinetic in the planar direction; eventually, carbon layers lift the particles and then trap them inside the tube walls.

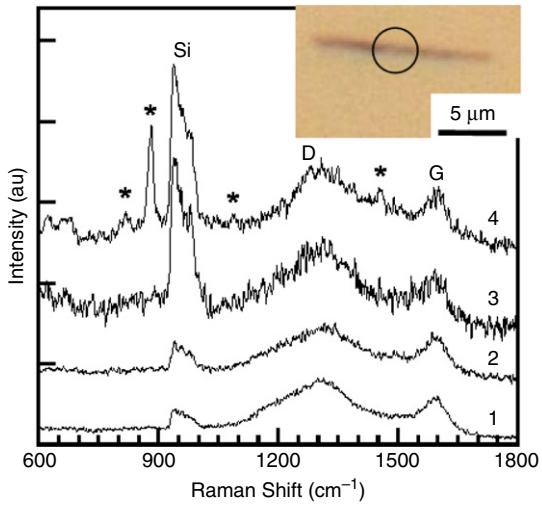

Figure 6. Raman spectra of (1) as-produced CNT; (2) as-produced CNT with glycine; (3) CNT with Au particles embedded in the walls; and (4) CNT with Au particles embedded in the walls with glycine. The inset shows an optical image of the actual CNT (diameter ∼200 nm) from which spectrum 4 was recorded on a Si surface. The empty circle represents the spot size of the laser beam.

(This figure is in colour only in the electronic version)

available at stacks.iop.org/Nano/18/155305), similarly to that previously reported for nickel nanoparticles [5].

3.2. Growth mechanism

TEM and SEM results both show that the nanoparticles are lifted from the template pore walls, and embedded in carbon deposited on the template during the CVD process. This appears to be counterintuitive because the particles were located on the template pore walls due to electrostatic attraction. However, our results are in agreement with those regarding the embedding of nickel oxide particles in the walls of nanotubes during corona discharge CVD [19]. The authors suggested that the detachment of the particles is due to the formation of nickel carbides with the subsequent diffusion of carbon in the carbide similar to the catalyst tip-growth mechanism of nanotubes [19]. Although this might be possible in the case of iron oxide, our results for gold nanoparticles cannot be explained by that mechanism. In addition, if the tip-growth was to occur, morphology similar to that in figure 5(a) should have been observed: a faster growth where the carbide particle is located and slower growth in areas between particles due to a concentration gradient of the diffusing carbon.

On the other hand, it is well known that graphite crystallites during CVD deposit with the basal plane parallel to the substrate [20]. Furthermore, upon graphitization, CVD nanotubes prepared in the same way as in this work but without particles, transformed in MWNTs with concentric walls [16]. Therefore, we suggest that carbon starts to deposit on the uncovered alumina template pore wall, further expanding along the pore wall (figure 5(b)). Once the carbon growing along the pore wall reaches a particle, it begins to lift it off from the substrate. The process continues, with the simultaneous formation of an equally thick layer of carbon on the nanoparticles that are still exposed in the cavity of the tubes (figure 4(c)).

3.3. Properties and potential applications

A droplet of CNT suspension in ethanol was placed on a clean silicon wafer and allowed to dry. Subsequently, a drop of an aqueous solution containing 1 mM of glycine, with pH 4 [21], was placed on top of the CNTs on the Si wafer. Since CVD nanotubes are hydrophilic [18], and can be filled with water [17], it is reasonable to assume that glycine solution filled the tube.

Raman spectra of CVD carbon nanotubes with and without Au nanoparticles (figure 6, curves 3 and 1, respectively) show no significant difference. The addition of CNTs without Au particles to the glycine solution yielded no enhancement (figure 6, curve 2), while signal enhancement was achieved only with nanotubes with gold particles embedded in the walls in glycine solution. Four additional peaks appeared at about 820, 880, 1085, and 1452 cm^{-1} (figure 6, curve 4). Because the concentration of glycine in the solution is too low to be observed by the conventional Raman technique [21], glycine outside the nanotube cannot yield any signal. Therefore, the SERS signal for glycine can only be coming from glycine molecules close to the Au nanoparticles, which are mainly inside the nanotube (figure 3). In addition, the thin layer of carbon covering the particles might be damping the signal, thus partially explaining the moderate glycine signal intensity. Comparison of these results to SERS of glycine in an Au colloid solution shows an upshift of about 5–10 cm^{-1} of the glycine peaks, possibly due the presence of the carbon layer between the gold and the glycine. This result opens the way to the development of nanotube-based SERS probes for the detection of extremely small amounts of

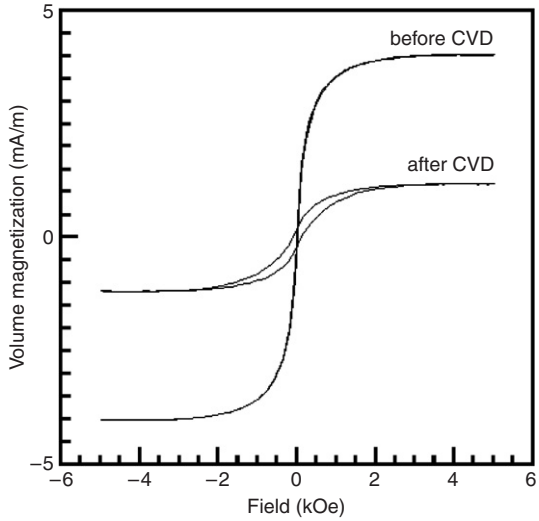

Figure 7. Typical magnetization curves of a fragment of alumina membrane before CVD, containing iron oxide nanoparticles, and after CVD, containing carbon nanotubes with iron-based particles embedded in the walls.

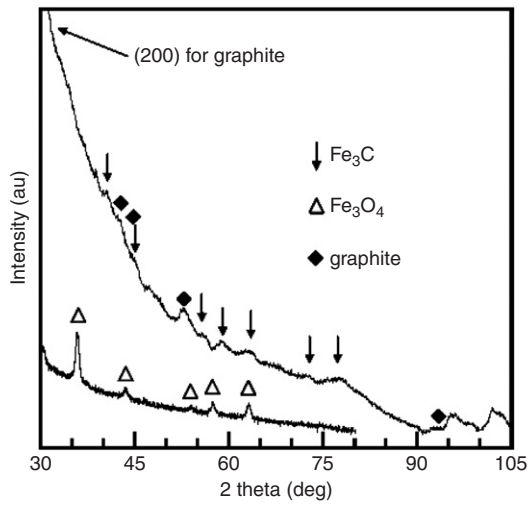

Figure 8. XRD patterns for the ferrofluid particles prior to CVD (lower curve) and for the CNTs with the iron/iron carbide particles embedded in their walls (upper curve).

biological and chemical components dispersed in liquids [22], or cellular research.

Fragments of membranes filled with magnetic particles before and after CVD treatment were placed in a magnetometer to measure the average magnetic properties. Typical volume magnetization curves for the membranes before and after CVD show a paramagnetic and a ferromagnetic behaviour, respectively (1.0 ml ferrofluid solution in 10 ml H_2O, figure 7).

The value of the volume saturation magnetization after CVD is about three times smaller than before CVD and the behaviour has changed from paramagnetic (no hysteresis) to ferromagnetic (with hysteresis). X-ray diffraction patterns show the presence of iron carbide (Fe_3C) after CVD and no peaks for Fe_3O_4 (figure 8) [23]. It is well known that iron carbide can be produced by hydrogen reduction of iron oxide to metallic iron and subsequent partial

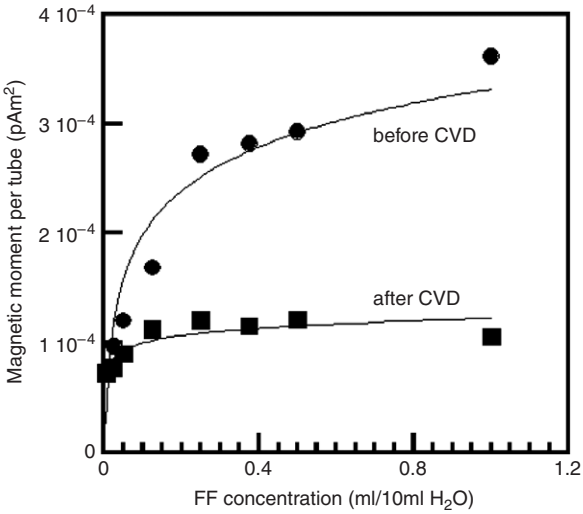

Figure 9. Magnetic moment per CNT before and after CVD synthesis as a function of the initial ferrofluid concentration.

carburization, with a metallic iron residue [24]. Hence, the reduction in saturation magnetization can be attributed to the replacement of some iron oxide by iron carbide, which has a saturation magnetization three orders of magnitude smaller than iron and two orders of magnitude smaller than Fe_3O_4 [23, 25]. The ferromagnetic behaviour is attributed to the residual metallic iron whose presence, although not visible in the XRD pattern, is also confirmed by the fact that MWNTs grow from iron-containing catalyst particles inside the CVD nanotubes (see supplementary information figure S1 available at stacks.iop.org/Nano/18/155305). Finally, EDS analysis of nanoparticles from which MWNTs originate shows peaks for carbon and iron alone, while EDS for larger particle agglomerates still show the presence of oxygen (see supplementary information figure S2 (a), (c), (e) and (d), respectively, available at stacks.iop.org/Nano/18/155305).

The magnetic moment per nanotube can be calculated as [8]:

$$m = M(d^2\pi)/(4\rho A), \tag{1}$$

where M is the volume magnetization, $d = 200$ nm is the average diameter of CVD nanotubes, $\rho = 0.35$ is the surface area fraction of the membrane occupied by nanotubes determined by image analysis of SEM of the membrane surface [18], and A is the area of the membrane fragment analysed. Comparison of the magnetic moments per tube before and after CVD is reported (figure 9), with a magnetic moment per tube of 3.5×10^{-16} A m^2 for the highest initial concentration of ferrofluid. Dividing this value by the magnetic moment of the iron oxide particles declared by the vendor, 4.48×10^{-20} A m^2, one can estimate the number of particles embedded in each nanotube, to be ~7000. This number is consistent with SEM observations of the tubes.

The highest average magnetic moment per tube achieved in the present work is only one order of magnitude smaller than the value obtained with 300 nm CVD nanotubes filled with the same magnetic particles after the CVD synthesis [8]. Those tubes have been manipulated by means of an external magnetic field, and we suggest that the magnetic tubes prepared in this work could also be manipulated in a similar way.

One key advantage, however, of the tubes prepared in this work is that the cavity of the CNT is empty, as is not always the case with tubes whose cavity is filled by magnetic particles. This could allow CNT alignment in the presence of a magnetic field without interfering with fluid flow inside the CNTs. These magnetically active tubes could also be manipulated through magnetic assembly in micro- and nano-devices [8], or loaded with drugs, driven to a specific location inside a cell or used for biosensing [26]. Magnetic manipulation of nanotubes with magnetic nanoparticles bonded to the outer structure of the nanotubes has already been suggested [4], although it is known that metallic nanoparticles can represent a health threat in a biological environment [27]. In the magnetic nanotubes synthesized in this work, metal particles are always covered by a carbon layer which does not allow direct chemical reaction or loss of particles in the environment.

When a particle is not completely embedded inside the nanotube wall with a part of it protruding inside the cavity of the nanotubes, additional carbon layers grow to cover the exposed surface. These structures occupy a considerable part of the hollow cavity of nanotubes, making this configuration very similar to a macroscopic static mixer used to modify flow dynamics and to mix or separate incoming fluids [28]. Such static mixing would be very important at the nanoscale, where the use of moving components is extremely difficult.

4. Conclusions

In summary, a one-step synthesis method to add multifunctionality to carbon nanotubes without altering the chemistry and structure of their surfaces has been developed. Nanoparticles of different sizes and compositions have been embedded in the nanotube walls during the nanotube growth. SERS of glycine using CNTs with Au particles in the walls has been demonstrated. Magnetic behaviour of the nanotubes with iron/iron oxide particles embedded in the walls has also been shown. Possible applications in fluid mixing and separation for the CNT with hillocks in the internal cavity of the tube with typical dimensions comparable to the bore of the tube will require further investigation.

Acknowledgments

The authors are grateful to Dr C Ni, University of Delaware, for assistance with the TEM, to Dr M Havel, Drexel University, for helpful discussions regarding SERS analysis. The authors acknowledge NSF for support through the NIRT grant CTS-0210579. ESEM and the Raman spectrometer are operated by the centralized Materials Characterization Facility of the A J Drexel Nanotechnology Institute. The vacuum furnace was donated by Solar Atmospheres, PA.

References

[1] Ebbesen T 1996 Wetting, filling and decorating carbon nanotubes *J. Phys. Chem. Solids* **57** 951–5
[2] Rakov E G 2006 Chemistry of carbon nanotubes *Nanomaterials Handbook* ed Y Gogotsi (Boca Raton, FL: CRC Press) pp 105–75
[3] Mu S-C, Tang H-L, Qian S-H, Pan M and Yuan R-Z 2006 Hydrogen storage in carbon nanotubes modified by microwave plasma etching and Pd decoration *Carbon* **44** 762–7
[4] Gao C, Li W, Morimoto H, Nagaoka Y and Maekawa T 2006 Magnetic carbon nanotubes: synthesis by electrostatic self-assembly approach and application in biomanipulations *J. Phys. Chem.* B **110** 7213–20
[5] Zhao X, Jiang P, Chu W, Mu S, Liu D, Song L, Liu L, Luo S, Zhang Z and Xiang Y 2006 The growth of carbon nanostructures in the channels of aligned carbon nanotubes *Carbon* **44** 1310–3
[6] Hattori Y, Watanabe Y, Kawasaki S, Okino F, Pradhan B K, Kyotani T, Tomita A and Touhara H 1999 Carbon-alloying of the rear surfaces of nanotubes by direct fluorination *Carbon* **37** 1033–8
[7] Kyotani T, Nakazaki S, Xu W H and Tomita A 2001 Chemical modification of the inner walls of carbon nanotubes by HNO_3 oxidation *Carbon* **39** 782–5
[8] Korneva G, Ye H, Gogotsi Y, Halverson D, Friedman G, Bradley J C and Kornev K G 2005 Carbon nanotubes loaded with magnetic particles *Nano Lett.* **5** 879–84
[9] Kim B M, Qian S and Bau H H 2005 Filling carbon nanotubes with particles *Nano Lett.* **5** 873–8
[10] Majumder M, Chopra N, Andrews R and Hinds B J 2005 Nanoscale hydrodynamics: enhanced flow in carbon nanotubes *Nature* **438** 44
[11] Cho S K, Fan S K, Moon H and Kim C J 2003 Creating, transporting, cutting, and merging liquid droplets by electrowetting-based actuation for digital microfluidic circuits *J. Microelectromech. Syst.* **12** 70–80
[12] Riegelman M, Liu H and Bau H H 2006 Controlled nano-assembly and construction of nanofluidic devices *J. Fluids Eng.* **128** 6–13
[13] Turkevich J, Stevenson P C and Hillier J 1951 A study of the nucleation and growth processes in the synthesis of colloidal gold *Discuss. Faraday Soc.* **11** 55–75
[14] McFarland A D, Haynes C L, Mirkin C A, Van Duyne R P and Godwin H A 2004 Color my nanoworld *J. Chem. Educ.* **81** 544A
[15] Kyotani T, Tsai L F and Tomita A 1995 Formation of ultrafine carbon tubes by using an anodic aluminium-oxide film as a template *Chem. Mater.* **7** 1427–8
[16] Mattia D, Rossi M P, Kim B M, Korneva G, Bau H H and Gogotsi Y 2006 Effect of graphitization on the wettability and electrical conductivity of CVD carbon nanotubes and films *J. Phys. Chem.* B **110** 9850–5
[17] Rossi M P, Ye H, Gogotsi Y, Babu S, Ndungu P and Bradley J C 2004 Environmental scanning electron microscopy study of water in carbon nanopipes *Nano Lett.* **4** 989–93
[18] Mattia D, Bau H H and Gogotsi Y 2006 Wetting of CVD carbon films by polar and non-polar liquids and implications for carbon nanopipes *Langmuir* **22** 1789–94
[19] Yu K-l, Zou J-j, Ben Y-h, Zhang Y-p and Liu C-j 2006 Synthesis of NiO-embedded carbon nanotubes using corona discharge enhanced chemical vapour deposition *Diamond Relat. Mater.* **15** 1217–22
[20] Pierson H O 1999 *Handbook of Chemical Vapor Deposition (CVD)* 2nd edn (Park Ridge, NJ: Noyes Publications)
[21] Dou X, Jung Y M, Cao Z Q and Ozaki Y 1999 Surface-enhanced Raman scattering of biological molecules on metal colloid II: effects of aggregation of gold colloid and comparison of effects of pH of glycine solutions between gold and silver colloids *Appl. Spectrosc.* **53** 1440–7
[22] Pieczonka N P W and Aroca R F 2005 Inherent complexities of trace detection by surface-enhanced Raman scattering *Chem. Phys. Chem.* **6** 2473–84
[23] Zhao X Q, Liang Y, Hu Z Q and Liu B X 1996 Oxidation characteristics and magnetic properties of iron carbide and iron ultrafine particles *J. Appl. Phys.* **80** 5857–60
[24] Hofer L J E and Cohn E M 1959 Saturation magnetization of iron carbides *J. Am. Chem. Soc.* **81** 1576–82

[25] Lide D R (ed) 2004 *Handbook of Chemistry and Physics* 85th edn (Boca Raton, FL: CRC Press)
[26] Graham D L, Ferreira H A and Freitas P P 2004 Magnetoresistive-based biosensors and biochips *Trends Biotechnol.* **22** 455–62
[27] Smart S K, Cassady A I, Lu G Q and Martin D J 2006 The biocompatibility of carbon nanotubes *Carbon* **44** 1034–47
[28] Fradette L, Li H-Z, Choplin L and Tanguy P 2006 Gas/liquid dispersions with a SMX static mixer in the laminar regime *Chem. Eng. Sci.* **61** 3506–18